HHS Public Access

Author manuscript

Mucosal Immunol. Author manuscript; available in PMC 2013 January 01.

Published in final edited form as:

Mucosal Immunol. 2012 July ; 5(4): 397–408. doi:10.1038/mi.2012.17.

Mucus clearance, MyD88-dependent and MyD88-independent immunity modulate lung susceptibility to spontaneous bacterial infection and inflammation

Alessandra Livraghi-Butrico[1], **E. Jane Kelly**[1], **Erich R. Klem**[1], **Hong Dang**[1], **Matthew C. Wolfgang**[1,2], **Richard C. Boucher**[1], **Scott H. Randell**[1], and **Wanda K. O'Neal**[1]

[1]Cystic Fibrosis/Pulmonary Research and Treatment Center, School of Medicine, The University of North Carolina at Chapel Hill, 7011 Thurston Bowles Building, Chapel Hill, NC 27599-7248, USA

[2]Department of Microbiology and Immunology, The University of North Carolina at Chapel Hill, 7011 Thurston Bowles Building, Chapel Hill, NC 27599-7248, USA

Abstract

It has been postulated that mucus stasis is central to the pathogenesis of obstructive lung diseases. In *Scnn1b*-transgenic (*Scnn1b*-Tg$^+$) mice, airway-targeted overexpression of the epithelial Na^+ channel β subunit causes airway surface dehydration, which results in mucus stasis and inflammation. Bronchoalveolar lavage from neonatal *Scnn1b*-Tg$^+$ mice, but not wild-type littermates, contained increased mucus, bacteria, and neutrophils, which declined with age. *Scnn1b*-Tg$^+$ mice lung bacterial flora included environmental and oropharyngeal species, suggesting inhalation and/or aspiration as routes of entry. Genetic deletion of the Toll/Interleukin-1 receptor adapter molecule MyD88 in *Scnn1b*-Tg$^+$ mice did not modify airway mucus obstruction, but caused defective neutrophil recruitment and increased bacterial infection, which persisted into adulthood. *Scnn1b*-Tg$^+$ mice derived into germ-free conditions exhibited mucus obstruction similar to conventional *Scnn1b*-Tg$^+$ mice and sterile inflammation. Collectively, these data suggest that dehydration-induced mucus stasis promotes infection, compounds defects in other immune mechanisms, and alone is sufficient to trigger airway inflammation.

INTRODUCTION

Respiratory health is maintained by an integrated network of innate and adaptive defense mechanisms. At the airway surface, mechanical mucus clearance is largely responsible for efficient removal of noxious stimuli, and mucus stasis has been suggested to produce airway lung diseases, including cystic fibrosis (CF), primary ciliary dyskinesia (PCD), and chronic obstructive pulmonary disease (COPD). Effective mucus clearance relies upon multiple

Corresponding author: Alessandra Livraghi-Butrico, Ph.D., University of North Carolina at Chapel Hill, Cystic Fibrosis/Pulmonary Research and Treatment Center, CB#7248 Thurston Bowles Bldg. Room # 6029, Chapel Hill, NC 27599, Phone: 919-843-1097, Fax: 919-966-5178, alessandra_livraghi@med.unc.edu.

Conflict of interest: The authors have no conflicting financial interests.

processes, e.g., epithelial ion and water transport, mucin secretion, ciliary beat, phasic airway motion, and cough [1]. Experimentally, mucus stasis has been achieved in mice by airway-targeted overexpression of the epithelial Na^+ channel β subunit (βENaC, encoded by the *Scnn1b* gene) [2]. In *Scnn1b*-transgenic (*Scnn1b*-Tg^+) mice, airway epithelial Na^+ hyperabsorption causes a depletion of airway surface liquid and an increase in mucus concentration [2], which is predicted to impair mucus clearance. Indeed, *Scnn1b*-Tg^+ mice exhibit mucus stasis and airway inflammation, which emerges in the neonatal period and produces a pathology resembling human CF/chronic bronchitis [2,3].

Although *Scnn1b*-Tg^+ mice exhibit delayed clearance of instilled bacteria [2] and chronic neutrophilic inflammation [3], the initial studies failed to detect spontaneous bacterial infection, a hallmark of CF lung disease [4] and an important component of COPD exacerbations [5]. This observation suggested that mucus stasis could produce inflammation without infection, i.e., sterile inflammation. However, the original microbiological studies were conducted only in adult mice and did not take into account the role of normal developmental processes, including maturation of innate and adaptive immunity [6,7] and transient abundance of mucous secretory cells [8,9], which likely play a role in the evolution of lung pathology in *Scnn1b*-Tg^+ mice. Moreover, static airway mucus creates a microaerophilic/hypoxic environment [10], which may favor the growth of bacterial species not detectable in the conventional aerobic bacterial cultures performed in the original studies of *Scnn1b*-Tg^+ mice.

Accordingly, we initiated a series of longitudinal studies designed to explore the interactions between mucus clearance and host defense in *Scnn1b*-Tg^+ mice. First, we tested the hypothesis that neonatal *Scnn1b*-Tg^+ mice are more susceptible to spontaneous bacterial infection than adult mice, due to the combination of defective mucus clearance, likely compounded by the transient increase in mucin production that occurs in the early postnatal period [8], and immature immune defenses. Thus, we measured bacterial colony forming units (CFUs) in bronchoalveolar lavage (BAL) as a function of age utilizing bacterial culture conditions that permitted detection of non-fastidious aerobes and microaerophilic bacteria. Second, we hypothesized that mechanical mucus clearance interacts with other developmentally regulated cellular defense mechanisms, e.g., Toll-like receptors (TLRs) [11,12], which could trigger airway inflammation in response to noxious stimuli accumulating in static mucus. Thus, we longitudinally evaluated whether components of *Scnn1b*-Tg^+ lung pathogenesis were dependent on Toll/Interleukin-1 receptor domain adapter protein myeloid differentiation factor 88 (MyD88), which mediates signaling through several TLRs [13] and is critical for early post-natal immunity [14,15]. Finally, to test whether live bacteria were necessary to trigger pulmonary inflammation due to airway surface dehydration and mucus stasis, we generated germ-free *Scnn1b*-Tg^+ mice and characterized their lung phenotype.

RESULTS

Scnn1b-Tg$^+$ mice routinely exhibit spontaneous bacterial infection during the neonatal period but are inflamed throughout life

The first goal of this study was to determine whether airway surface dehydration and mucus stasis promoted spontaneous bacterial infection in *Scnn1b*-Tg$^+$ mice. Longitudinal analysis of BAL from congenic C57BL6/N *Scnn1b*-Tg$^+$ and wild-type (WT) littermates revealed no culturable bacteria in WT mice, whereas the majority of *Scnn1b*-Tg$^+$ pups harbored intrapulmonary bacteria (Figure 1a). As *Scnn1b*-Tg$^+$ mice aged, both the proportion of infected mice and the number of bacterial colony forming units (CFU) decreased.

Morphologically distinct bacterial colonies recovered from *Scnn1b*-Tg$^+$ mice were identified by ribosomal 16S gene sequencing (Figure 1b). *Scnn1b*-Tg$^+$ neonatal lung microflora included both Gram positive (mainly *Streptococcus* species and to lesser extent *Staphylococcus xylosus*, and *Rothia nasimurium*) and Gram negative bacteria (mainly *Pasturella pneumotropica* and *Actinobacillus muris*). Similar bacterial species were present in tissue homogenates of tongue and esophagus from 5 day-old mice, with no clear distinction between WT or *Scnn1b*-Tg$^+$ mice (Figure 1c, tongue and esophagus), whereas these bacteria were frequently detected in tracheal homogenates from 5 day-old *Scnn1b*-Tg$^+$ mice as compared to WT littermates (Figure 1c, trachea). The composition of the lung microflora in adult *Scnn1b*-Tg$^+$ mice differed from younger mice, featuring low levels of Gram positive bacteria, e.g., *Bacillus clausii* and *Bacillus pumilus* at 1 month and *Streptomyces* and *Staphylococcus lentus* at 7 months of age (Figure 1b), suggesting a process of selection/adaptation.

Longitudinal analysis of BAL inflammatory markers indicated that *Scnn1b*-Tg$^+$ mice exhibited an increased inflammatory infiltrate, predominantly neutrophilic, as compared to WT littermates at all ages (Figure 2). The relative increases in BAL neutrophils, KC and TNFα were more robust in neonatal mice (Figure 2b,e,f) when bacterial burden was highest. In contrast, the number of BAL macrophages and lymphocytes in the *Scnn1b*-Tg$^+$ mice increased with age (Figure 2a,d), and eosinophils peaked at 4–8 wks (Figure 2c). Macrophages were morphologically activated in both neonatal (5 day-old) and adult (4 week-old) *Scnn1b*-Tg$^+$ mice, as indicated by higher incidence of enlarged macrophages compared to WT littermates (Figure 2g,h).

Ablation of MyD88 signaling in Scnn1b-Tg$^+$ mice causes defective neutrophil recruitment and higher lung bacterial burden, but does not affect airway mucus obstruction

The temporal pattern of infection in *Scnn1b*-Tg$^+$ mice suggests the interaction of airway mucus clearance with other developmentally regulated innate immune components, e.g., MyD88-dependent TLR signaling. To test this hypothesis, we generated *Scnn1b*-Tg$^+$ and WT littermates (for this cross, referred to as *Scnn1b*-Tg$^-$) that were either MyD88-sufficient (MyD88$^{+/-}$) or MyD88-deficient (MyD88$^{-/-}$). When raised under controlled husbandry conditions (see Methods), survival of all *Scnn1b*-Tg$^+$ mice ranged between 75–100% (Figure 3a), reflecting the favorable effect of the C57Bl/6N genetic background [8] compared to the original C3H:C57 background, which had ~ 50% survival [2]. Importantly, survival of

MyD88$^{-/-}$;*Scnn1b*-Tg^{+} mice was significantly lower than MyD88$^{+/-}$;*Scnn1b*-Tg^{+} or the other genotypes (ANOVA, p = 0.004), indicating that combined *Scnn1b* transgene overexpression and MyD88 homozygous deletion had a detrimental effect.

Microscopic analysis of BAL cytospin preparations revealed rod- and cocci-shaped bacteria in association with mucus plugs in neonatal MyD88$^{-/-}$;*Scnn1b*-Tg^{+} mice, which were never observed in MyD88$^{+/-}$;*Scnn1b*-Tg^{+} mice, despite similar mucus plugs (Figure 3b). Quantification of bacterial burden revealed that MyD88$^{-/-}$;*Scnn1b*-Tg^{+} mice harbored significantly more bacteria than MyD88$^{+/-}$;*Scnn1b*-Tg^{+} mice at all time points, and infection persisted into adulthood, although its severity decreased with age (Figure 3c). In particular, heterozygosity for MyD88 was sufficient to protect mice not carrying the *Scnn1b* transgene (MyD88$^{+/-}$;*Scnn1b*-Tg^{-}) from spontaneous bacterial infection. Conversely, complete MyD88 deficiency (MyD88$^{-/-}$;*Scnn1b*-Tg^{-}) led to significant bacterial burden in neonatal mice, which decreased at post-natal day (PND) 8–10 and was undetectable in adult mice. In agreement with the data presented in Figure 1a, bacteria were present in BAL of all neonatal MyD88$^{+/-}$;*Scnn1b*-Tg^{+} mice, and were sporadically detected in adult mice.

The lung microflora of colonized mice from the MyD88$^{-/-}$ × *Scnn1b*-Tg^{+} cross (Figure 3d) was also more diverse than in C57BL/6N *Scnn1b*-Tg^{+} mice (Figure 1b). *Streptococcus* and *Klebsiella* species were prevalent, and *Staphylococcus*, *Proteus*, *Enterococcus*, and *Rothia* species were frequently detected but at lower density (Figure 3d). Of note, *Streptococcus*, *Klebsiella*, *Staphylococcus* and *Enterococcus* species persisted in MyD88$^{-/-}$;Scnn1b-Tg^{+} mice throughout adulthood.

A longitudinal analysis of BAL cell counts and inflammatory mediators was performed to assess the contribution of MyD88 signaling to lung inflammation. Notably, BAL neutrophil counts were lower in MyD88$^{-/-}$;*Scnn1b*-Tg^{+} versus MyD88$^{+/-}$;*Scnn1b*-Tg^{+} mice at all time points (Figure 4b). Macrophages constituted the predominant cell population in MyD88$^{+/-}$ and MyD88$^{-/-}$ mice not carrying the *Scnn1b* transgene (Figure 4a). Except for PND 10, when macrophages were increased, Myd88$^{-/-}$;*Scnn1b*-Tg^{+} mice exhibited macrophage numbers (Figure 4a) and morphological activation (Figure 4e) similar to Myd88$^{+/-}$;*Scnn1b*-Tg^{+} mice. Absence of MyD88 also reduced BAL eosinophils in 10 day-old *Scnn1b*-Tg^{+} mice and prevented the transient developmental eosinophilia in *Scnn1b*-Tg^{-} mice [8] (Figure 4c). Finally, BAL lymphocytes were sharply increased in Myd88$^{-/-}$;*Scnn1b*-Tg^{+} mice at PND 10, but waned afterwards (Figure 4d).

The inflammatory mediator profile of cell-free BAL (Figure 5) mirrored the changes in BAL cell composition. Myd88$^{-/-}$;*Scnn1b*-Tg^{+} mice exhibited reduced neutrophil chemoattractants (KC, LIX, MIP-2), granulocyte differentiation factors (G-CSF), and TNFα at PND 5 compared to Myd88$^{+/-}$;*Scnn1b*-Tg^{+} mice. Macrophage colony stimulating factor (M-CSF) was higher at PND 10 in Myd88$^{-/-}$;*Scnn1b*-Tg^{+} mice, paralleling higher BAL macrophages at this time point. MIP-1α, IL-6, GM-CSF, IL-1α, IL-1β, and MCP-1 were either at or below the lower limit of detection, and differences among groups failed to be significant or exhibit consistent trends (data not shown).

A longitudinal histological analysis was performed to test whether MyD88 deficiency modified the lung pathology in *Scnn1b*-Tg$^+$ mice (Figure 6). Absence of MyD88 did not alter the transient abundance of tracheal and bronchial mucous secretory cells normally observed postnatally [8,9] (Figure 6a,b). Myd88$^{+/-}$;*Scnn1b*-Tg$^+$ and Myd88$^{-/-}$;*Scnn1b*-Tg$^+$ mice exhibited comparable tracheal mucus plugging and mucous secretory cells in neonates (Figure 6a), a similar progression of mucus obstruction (from trachea to bronchi, Figure 6a,c), and equivalent air space enlargement (data not shown). However, 8 week-old Myd88$^{-/-}$;*Scnn1b*-Tg$^+$ mice had significantly more lymphoid aggregates than Myd88$^{+/-}$;*Scnn1b*-Tg$^+$ mice (Figure 6d), suggesting a response to a greater bacterial burden and/or alteration of adaptive immune responses.

Germ-free Scnn1b-Tg$^+$ mice are devoid of bacteria, but still develop mucus obstructive lung disease

To define the relative contributions of dehydrated mucus vs. neonatal bacterial infection to the development of obstructive airways disease, we derived *Scnn1b*-Tg$^+$ mice in a germ-free (GF) environment. As expected, BAL from GF *Scnn1b*-Tg$^+$ mice harvested at PND 5, when both incidence of infection and bacterial load are maximal in SPF *Scnn1b*-Tg$^+$ mice, was sterile (n=5). Adult GF *Scnn1b*-Tg$^+$ mice exhibited overt airway mucus obstruction and, strikingly, persistent inflammation (Figure 7a–c). Indeed, the overall lung pathology, as assessed by semi-quantitative histology score, was comparable in GF and SPF *Scnn1b*-Tg$^+$ mice, at both 10 days and 4 weeks of age (Figure 7d).

BAL longitudinal analysis revealed that 5–10 day-old GF *Scnn1b*-Tg$^+$ mice had more macrophages than their WT littermates (Figure 7e), which was not a feature of SPF *Scnn1b*-Tg$^+$ mice (Figure 2a). Although macrophage number in adult GF *Scnn1b*-Tg$^+$ mice normalized towards WT levels, GF *Scnn1b*-Tg$^+$ macrophages remained morphologically activated (Figure 7i). GF *Scnn1b*-Tg$^+$ mice had higher neutrophil counts compared to WT littermates at all time points (Figure 7f) and more eosinophils and lymphocytes in adult mice (Figure 7g-h). Of note, BAL neutrophil counts were lower in neonatal GF *Scnn1b*-Tg$^+$ mice compared to SPF *Scnn1b*-Tg$^+$ mice ($87 \pm 18\times10^3$ vs. $269 \pm 71\times10^3$ for GF and SPF 10 day-old mice, respectively, $p<0.05$), but did not differ in adult mice. As in the SPF environment, the BAL cytokine profile of GF *Scnn1b*-Tg$^+$ mice was characterized by elevated neutrophil-related mediators (KC, LIX, and G-CSF), whereas, unlike SPF *Scnn1b*-Tg$^+$ mice, TNFα was not elevated compared to WT littermates (Figure 8a).

Because sterilized feed and bedding in GF conditions are not free of bacterial products, we tested whether environmental LPS, trapped after inhalation by static airway mucus, could be responsible for stimulating inflammation in GF *Scnn1b*-Tg$^+$ mice. As expected, the level of LPS in unfractionated BAL from 5 day-old SPF *Scnn1b*-Tg$^+$ was significantly higher than in WT littermates, but LPS was barely detectable and equivalent in GF *Scnn1b*-Tg$^+$ mice and WT littermates (Figure 8b). Thus, the inflammation observed in GF *Scnn1b*-Tg$^+$ mice appears to be independent of both live bacteria and at least one major bacterial product (LPS).

DISCUSSION

In the respiratory tract, effective host defense depends primarily upon rapid mechanical clearance of inhaled noxious agents [16]. The paradigm that defective mucus clearance favors bacterial infections of the airways is widely accepted [1], but has never been rigorously tested, nor has the interplay between mucus clearance and other innate defense mechanisms been explored. We used an *in vivo* model of abnormal mucus clearance, i.e., the *Scnn1b*-Tg$^+$ mouse, to explore the mechanisms involved in acquisition versus protection from airway bacterial infections.

Spontaneous bacterial infections are rarely reported in mouse models and usually occur in immunocompromized strains [17–19]. Our longitudinal studies indicate that defective mucus clearance caused a breach in host defense resulting in an age-dependent presence of bacteria in the lungs (Figure 1a). This presence likely constitutes an “infection”, as indicated by higher neutrophils and TNFα in BAL from SPF *Scnn1b*-Tg$^+$ mice (Figure 2b,f) compared to GF *Scnn1b*-Tg$^+$ mice which have similar mucus obstruction but no bacteria (Figures 7f and 8a). As occurs in CF [10], the infection in *Scnn1b*-Tg$^+$ mice appears to be centered on the airways (Figure 1c, trachea, and Figure 3b, airway mucus). We speculate that the bacterial density (10^3/lung) likely reprises that observed in human muco-obstructive airway infections. Specifically, we estimated that the mucus volume in neonatal *Scnn1b*-Tg$^+$ mice is ~ 1 μl (see Methods), producing a density of 10^6 bacteria/ml, a value typical for sputum samples in CF subjects [20].

The decrease in lung bacterial burden as *Scnn1b*-Tg$^+$ mice aged is likely due to the postnatal maturation of innate [21] and adaptive [7] immunity, including changes in pattern recognition receptor expression [11,12], neutrophils [22] and antigen presenting cell functions [23], as well as changes in airway mucous secretory cell number/secretions [8,9,24,25]. Moreover, in mouse airways the density of airway ciliated cells increases with age [26] and maximal mucus transport rates are generated after PND 9 [27], partially offsetting the clearance defect due to mucus dehydration in *Scnn1b*-Tg$^+$ mice.

The bacterial species most prevalent in the lungs of *Scnn1b*-Tg$^+$ mice during the neonatal period also populated the mouse tongue and esophagus (Figure 1c), suggesting the oropharynx as the portal of entry. We speculate that while aspiration occurred in both WT and *Scnn1b*-Tg$^+$ mice, infection selectively affected *Scnn1b*-Tg$^+$ mice due to the poor clearance of aspirated contents. CF patients also exhibit concordant bacterial genotypes in the upper and lower airways [28–30], indicating aspiration as a likely mechanism of spread in human diseases associated with pulmonary mucus stasis.

The shift in bacterial species between neonatal and adult *Scnn1b*-Tg$^+$ mice may indicate that, after clearing the initial infection, *Scnn1b*-Tg$^+$ mice became susceptible to intermittent infection with species already present in the cage and/or oral environment. Alternatively, bacterial competition in the mucus niche may have favored the species recovered in older mice. Regardless, these data highlight a feature of this model which should be helpful for studying the longitudinal pathogenesis of chronic lung diseases characterized by persistent/recurrent bacterial infection [31].

Certain caveats apply to our microbiologic studies. First, mice housed in SPF facilities are not exposed to highly infectious murine pathogens, which may be more successful in establishing persistent infection in *Scnn1b*-Tg^{+} mice. Second, BAL sampling might have not harvested all bacteria, but it was preferred over lung homogenization which was found to inhibit growth of the isolated species. Third, bacterial detection was limited to species capable of growth under the specific culture conditions used, which were not permissive for strict anaerobes and fastidious aerobes. Future studies should focus on exposure to selected pathogens and more sophisticated culture-independent methods suitable to detect small numbers of bacteria, i.e., emulsion PCR and 454 pyrosequencing.

Our studies also demonstrated that other mucosal defense mechanisms modulate the response to airway bacterial infection due to defective mucus clearance. Studies designed to identify ancillary protective mechanisms revealed that MyD88-dependent innate immunity is key in determining the severity of airway bacterial infections in *Scnn1b*-Tg mice. In neonatal mice, MyD88 deficiency in the absence of mucus stasis (MyD88$^{-/-}$;*Scnn1b*-Tg^{-} mice) produced bacterial burdens comparable to those caused by mucus obstruction alone (MyD88$^{+/-}$;*Scnn1b*-Tg^{+} mice) (Figure 3c), whereas the presence of both MyD88 deficiency and mucus stasis (MyD88$^{-/-}$;*Scnn1b*-Tg^{+} mice) produced an additive effect, suggesting that the two defense mechanisms operate independently. Of note, the greater bacterial burden in neonatal MyD88$^{-/-}$;*Scnn1b*-Tg^{+} mice compared to MyD88$^{+/-}$;*Scnn1b*-Tg^{+} mice was not associated with increased mucus obstruction or mucous secretory cells (Figure 6a–c), indicating that MyD88 deletion predominantly affected the immune functions of inflammatory [32] and epithelial cells [33].

The sensitivity of MyD88$^{-/-}$ mice to bacterial infection differs depending on the microorganism studied [34], but is generally regarded as “broad”. MyD88 deletion prevents signaling through TLR 1, 2, 4, 5, 7, and 9 and blunts immune responses by impairing neutrophil chemotaxis (Figure 4b) and secretion of inflammatory mediators, such as KC, MIP-2, CXCL5/LIX (Figure 5). However, both MyD88$^{-/-}$;*Scnn1b*-Tg^{-} mice and MyD88$^{-/-}$;*Scnn1b*-Tg^{+} mice exhibited reduced bacterial burdens as a function of age (Figure 3c), indicating the maturation of MyD88-independent protective mechanisms [13,16,35–37]. Nonetheless, the higher and persistent bacterial burden in adult MyD88$^{-/-}$;*Scnn1b*-Tg^{+} mice suggests that the MyD88-independent mechanisms were insufficient to completely overcome two additive defects in mucosal defense.

The studies described above highlight the complex interplay between mucus obstruction, infection, and inflammation in our model. The persistence of lung neutrophilia in adult *Scnn1b*-Tg^{+} mice (Figure 2b) could reflect the presence of non-culturable bacteria. Alternatively, airway mucus stasis *per se* could contribute to the inflammatory response observed in muco-obstructive lung diseases by impairing clearance of noxious stimuli. To distinguish between these two hypotheses, we generated GF *Scnn1b*-Tg^{+} mice, which were reared in a low-endotoxin environment (Figure 8b). Notably, adult GF *Scnn1b*-Tg^{+} mice exhibited lung inflammation and histopathology comparable to SPF *Scnn1b*-Tg^{+} mice (Figure 7), supporting the hypothesis that mucus stasis *per se* can lead to inflammation by trapping non-infectious, noxious materials.

As LPS levels were minimal in the GF environment (Figure 8b), we speculate that other stimuli contributed to macrophage activation (Figure 7i) and neutrophil recruitment (Figure 7f) in GF *Scnn1b*-Tg$^+$ mice. Beside inhaled noxious stimuli, necrotic bronchial epithelial cells transiently present in 3 day-old *Scnn1b*-Tg$^+$ mice [3] could also contribute to the sterile inflammation observed in *Scnn1b*-Tg$^+$ mice. We speculate that once initiated by poor clearance of toxic materials, the inflammatory process is perpetuated by the retention of stimuli causing macrophage activation and the sequelae of neutrophil recruitment, including secondary necrosis [38] and release of other chemoattractants, e.g., high-mobility group box 1 and PGP [39].

Additional features of mice reared in the GF environment were noted. GF mice still exhibit the transient neonatal surge in mucous secretory cells and eosinophils described for SPF mice [8] (Figure 7d,g). Furthermore, neonatal GF WT mice had fewer neutrophils (Figure 7f) than neonatal SPF WT mice (Figure 2b), consistent with the notion that normal airways may not be completely sterile and intrapulmonary bacteria help guide immune development [40]. Indeed, the absence of environmental bacteria might affect the overall immune response to airway mucus stasis, as suggested by the higher number of macrophages recovered in neonatal GF vs. SPF *Scnn1b*-Tg$^+$ mice (Figures 7e and 2a). Finally, both SPF and GF *Scnn1b*-Tg$^+$ mice develop bronchial-associated lymphoid tissue (BALT) (Figure 7d and [8]), which is usually thought to result from TLR stimulation [41] and whose incidence correlates with worsening airflow obstruction in COPD patients [42]. The observation that both MyD88$^{-/-}$; *Scnn1b*-Tg$^+$ mice and GF *Scnn1b*-Tg$^+$ mice exhibit lymphoid aggregates suggests that neither MyD88 signaling nor bacterial stimulation is required for this response in the context of airway mucus stasis.

The hypothesis that CF is characterized by intrinsic lung inflammation in the absence of bacterial infection is controversial [43,44], and novel animal models have been generated to better understand the critical phases of disease onset and progression [45,46]. Although we did not perform BAL studies on prenatal *Scnn1b*-Tg$^+$ mice, whose airways are not exposed to bacteria or bacterial products, previous studies reported that the concentration of KC and MIP-2 in lung homogenates from newborn (PND 1) *Scnn1b*-Tg$^+$ mice was not different from WT littermates [2], whereas an inflammatory infiltrate was clearly present in *Scnn1b*-Tg$^+$ mice just a few days later (PND3), in conjunction with tracheal mucus plugging [3,47], suggesting that the inflammatory response develops as a consequence of airway mucus obstruction. Collectively, our data from the GF and SPF *Scnn1b*-Tg$^+$ mice suggest that mucus stasis *per se* produces airway inflammation and that mucus stasis results in susceptibility to infection by bacteria aspirated from the oropharynx. Due to its unique phenotype and the amenability to complex genetic and environmental manipulations, the *Scnn1b*-Tg$^+$ mouse model has allowed us to probe the interactions of abnormal mucus clearance and other layers of lung defense, e.g., MyD88-dependent pathways. Our data suggest that stagnant mucus can initiate both the inflammatory and infectious components of obstructive lung diseases and thus, is a primary therapeutic target. As such, therapies aimed at promoting mucus clearance would provide three interconnected benefits, namely to alleviate inflammation, eradicate infection, and restore immune homeostasis.

METHODS

Mice

Mice were housed in a specific pathogen free (SPF) facility at the University of North Carolina at Chapel Hill. Congenic C57Bl6/N *Scnn1b*-Tg^{+} mice were generated by backcrossing C3:B6 *Scnn1b*-Tg^{+} mice line 6608 [2] with C57Bl/6N mice (Taconic, Hudson, NY) for more than 12 generations. Mice were housed in hot-washed, individually ventilated micro-isolator cages with corn cob bedding, on a 12-hour day/night cycle, fed regular chow and given water *ad libitum*. MyD88$^{-/-}$ mice [B6.129P2-Myd88^{tm1Aki} [48], kindly provided by Dr. Shizuo Akira, Osaka University, through Dr. Jonathan Serody, University of North Carolina at Chapel Hill] were bred with C57Bl6 *Scnn1b*-Tg^{+} mice to obtain experimental animals of four predicted genotypes with expected Mendelian distribution of 25% each: MyD88$^{+/-}$;*Scnn1b*-Tg^{-}, MyD88$^{-/-}$;*Scnn1b*-Tg^{-}, MyD88$^{+/-}$;*Scnn1b*-Tg^{+}, and MyD88$^{-/-}$;*Scnn1b*-Tg^{+}. This breeding strategy generated control mice heterozygous for MyD88, which were not expected to be different from MyD88$^{+/+}$ mice, and gave the advantage that experimental animals of all four genotypes were littermates and shared an identical environment. Our first attempt to establish this colony and monitor survival by early toe excision (PND 2–3) was unsuccessful as MyD88$^{-/-}$ mice rapidly died, likely due to susceptibility to infection after early toeing. To increase survival, breeder pairs were housed in “cleaner conditions”, i.e., cages with autoclaved TEK-FRESH bedding (Harlan) changed weekly, and were given autoclaved food and antibiotic-supplemented water (sulfamethoxazole 0.64 mg/ml and trimethoprim, 0.13 mg/ml) until the dams gave birth. Pups were toed for identification and genotyping at PND 5. Germ-free *Scnn1b*-Tg^{+} mice were generated in the National Gnotobiotic Rodent Resource Center at UNC. Germ-free rodents are axenic, with no detectable bacteria, yeast, molds, parasites or viruses (except retroviruses). To monitor the sterility of the isolator containing the GF *Scnn1b*-Tg^{+} mouse colony, samples of fresh feces, mouth/paws/cages swabs, and drinking water were collected from breeders and holding mice every time the port was open. Collected samples were tested for the presence of contaminating bacteria by plating onto sheep blood agar, growth in fluid thioglycollate medium (FTG), and Gram staining. Regardless of port opening, all isolators were periodically monitored (every other month) through Gram staining and 16S PCR on sampled feces. The isolator containing the GF *Scnn1b*-Tg^{+} mice colony never suffered a breach in germ-free status, and we studied mice from different litters at different ages, over a several months period. All animal studies were approved by the Institutional Animal Care and Use Committee of the University of North Carolina at Chapel Hill and performed according to the principles outlined by the Animal Welfare and the National Institutes of Health guidelines for the care and use of animals in biomedical research.

Bronchoalveolar lavage (BAL), differential cell counts, lung histology, and macrophage size

For 10 day-old or older mice, we obtained both BAL and lung histology from each animal, as previously described [8]. Due to their small size, 5 day-old pups were subject to either whole lung BAL or tissue harvesting. Macrophage size was determined by measuring the surface area of 60–80 macrophages/mouse. Cytospin preparations were photographed with a Leica DMIRB inverted microscope interfaced with a Micro Publisher 3.3 color camera (Q-

Imaging, Surrey, BC, Canada) at 20× magnification and macrophage area was determined using the calibrated freehand selection tool of Image J analysis software (NIH, Bethesda). Histology specimens were scored by an investigator blinded to genotype using a semi-quantitative scoring system, as described previously [8].

Cytokine profile

Mouse TNFα, KC, MIP-2, MIP-1α, M-CSF, MCP-1, LIX, IL-6, IL-1α, IL-1β, GM-CSF, and G-CSF were measured in cell-free BAL using a Luminex-based assay (EMD Millipore, Billerica, MA), according to the manufacturer instructions.

Bacteriology

BAL was performed aseptically, inserting the cannula by tracheotomy in the lower portion of the trachea, to avoid oropharyngeal bacteria. Whole lungs were lavaged 4 times, using a weight-based formula [8] and fractions pooled. Serial BAL dilutions were plated onto Columbia anaerobe sheep blood agar (Becton Dickinson, NJ) and incubated in a candle jar to facilitate the growth of microaerophilic bacteria. Plates were incubated at 37°C for 24 hours, and colony forming units (CFU) were enumerated and classified based on their morphology. Individual colonies representative of each morphologic group were expanded and processed for molecular identification. For detection of bacteria in tissue homogenates, tongue, esophagus, trachea and lungs were dissected from 5 day-old mice and homogenized in 1 ml of sterile Dulbecco's phosphate-buffered saline (D-PBS, Sigma, MO) using a Tissue Tearor (Biospec products, OK) on ice. Serial dilutions were plated and processed as described above.

Molecular identification of bacterial species

Bacterial DNA was extracted using the FastDNA SPIN Kit, lysing Matrix B protocol (MP Biomedicals, OH), according to manufacturer's instructions. The ribosomal 16S gene was amplified by PCR using HPLC-purified primers (forward 5′ AGAGTTTGATC(A + C)TGGCTCAG 3′, reverse 5′ TACGG(C+T)TACCTTGTTACGACTT 3′) and the following PCR conditions: denaturing 95°C for 5 min; 35 cycles of amplification (95°C for 20 sec, 51°C for 20, 72°C for 1 min and 10 sec); 72°C for 8 min. Primers and dNTPs were removed from the PCR product by digestion with exonuclease I and shrimp alkaline phosphatase (ExoSAP-IT, USB Corp., OH). The PCR product was sequenced using both forward and reverse primers (Genewiz, NJ). Bacterial identities were inferred from the degree of alignment of the ribosomal 16S gene sequences with existing databases (NCBI Nucleotide collection, excluding "models" and "uncultured/environmental sample sequences"), using the NCBI Basic Local Alignment Search Tool (BLAST).

LPS assay

Limulus amebocyte lysate assay was performed on unfractionated BAL from 5 day-old WT and *Scnn1b*-Tg$^+$ mice using the Pyrochrome kinetic method, according to manufacturer instructions (Associates of Cape Cod, Inc. MA). The assay was performed under conditions that allowed cumulative detection of both LPS and β-glucan.

Estimate of mucus volume

Mucus volume was calculated from the adult mouse ASL volume of 2.27 μl [49] and the adult/pup scaling factor of 2, obtained by dividing the average tracheal length or diameter in 20 g vs. 3 g mice. Measurements were courtesy of Dr. Barbara Grubb, UNC Chapel Hill.

Statistical analyses

Statistical analyses were performed using SigmaStat 3.1 or JMP 8.0.2. Survival curves were compared using Kaplan-Meier log rank analysis and Holm-Sidak multiple comparison. All numeric values were log10 transformed with an offset of +1 before inferential statistical analyses. Comparisons between measurements from 2 groups with significant difference in variances were performed using Student t test assuming non-equal variance, or non-parametric Wilcoxon rank-sum test. Comparison between multiple groups were performed using one-way analysis of variance (ANOVA) and differences among the group means were assessed by Tukey-Kramer post-hoc test for multiple test correction. For inferential statistics, $p<0.05$ was considered statistically significant and "n" represents the number of animals in each experimental group. Data presented in plots with error bars are expressed as mean ± SEM. Distribution of macrophage sizes between control (WT or MyD88$^{+/-}$;*Scnn1b*-Tg^{-}) and test groups were performed by determining the 90% threshold in the control group, and comparing the proportion of cells in the test group beyond the threshold. Statistical significance between the proportions of cells that passed the threshold in the test group vs. control group (10%) was evaluated using χ^2 test.

Acknowledgments

The authors thank: The authors thank: Nanette B. Fulcher for advice in microbiology techniques and data analysis; Kimberly Burns, Donald Joyner and Tracy Eldred for technical assistance with histology; Kristy Terrell and Kimberly Brassard for assistance with bacterial species identification; Rodney Gilmore for assistance with mouse genotyping; the UNC Michael Hooker Microscopy Facility, funded by an anonymous private donor; the Clinical Proteomics Laboratory at the UNC Thurston Arthritis Research Center and the Immunotechnology Core at the UNC Center for Gastrointestinal Biology and Disease for Luminex assays; Maureen A. Bower, Kathy Mohr, and Jamison D. Cameron in the UNC Center for Gastrointestinal Biology and Disease Gnotobiotic Core directed by Dr. B. Sartor and supported by NIH grant P30 DK34987 for generating and maintaining the germ-free *Scnn1b*-Tg mouse colony. The studies were supported by grant RANDEL07P0 awarded to S.H. Randell by the Cystic Fibrosis Foundation, and by the Cystic Fibrosis Research Development Program grant RDP R026, and National Institute of Health P30 DK065988 and P50 HL060280 to W.K. O'Neal and R.C. Boucher.

LITERATURE CITED

1. Randell SH, Boucher RC. Effective mucus clearance is essential for respiratory health. Am J Respir Cell Mol Biol. 2006; 35:20–8. [PubMed: 16528010]
2. Mall M, Grubb BR, Harkema JR, O'Neal WK, Boucher RC. Increased airway epithelial Na+ absorption produces cystic fibrosis-like lung disease in mice. Nat Med. 2004; 10:487–93. [PubMed: 15077107]
3. Mall MA, et al. Development of chronic bronchitis and emphysema in beta-epithelial Na+ channel-overexpressing mice. Am J Respir Crit Care Med. 2008; 177:730–42. [PubMed: 18079494]
4. Hauser AR, Jain M, Bar-Meir M, McColley SA. Clinical significance of microbial infection and adaptation in cystic fibrosis. Clin Microbiol Rev. 2011; 24:29–70. [PubMed: 21233507]
5. Sethi S. Infection as a comorbidity of COPD. Eur Respir J. 2010; 35:1209–15. [PubMed: 20513910]
6. Levy O. Innate immunity of the newborn: basic mechanisms and clinical correlates. Nat Rev Immunol. 2007; 7:379–390. [PubMed: 17457344]

7. Adkins B, Leclerc C, Marshall-Clarke S. Neonatal adaptive immunity comes of age. Nat Rev Immunol. 2004; 4:553–64. [PubMed: 15229474]
8. Livraghi A, et al. Airway and lung pathology due to mucosal surface dehydration in {beta}-epithelial Na+ channel-overexpressing mice: role of TNF-{alpha} and IL-4R{alpha} signaling, influence of neonatal development, and limited efficacy of glucocorticoid treatment. J Immunol. 2009; 182:4357–67. [PubMed: 19299736]
9. Roy MG, et al. Mucin Production During Pre- and Post-Natal Mouse Lung Development. Am J Respir Cell Mol Biol. 2011
10. Worlitzsch D, et al. Effects of reduced mucus oxygen concentration in airway Pseudomonas infections of cystic fibrosis patients. J Clin Invest. 2002; 109:317–25. [PubMed: 11827991]
11. Sadeghi K, et al. Immaturity of infection control in preterm and term newborns is associated with impaired toll-like receptor signaling. J Infect Dis. 2007; 195:296–302. [PubMed: 17191175]
12. Al-Hertani W, Yan SR, Byers DM, Bortolussi R. Human newborn polymorphonuclear neutrophils exhibit decreased levels of MyD88 and attenuated p38 phosphorylation in response to lipopolysaccharide. Clin Invest Med. 2007; 30:E44–53. [PubMed: 17716541]
13. Kumar H, Kawai T, Akira S. Toll-like receptors and innate immunity. Biochem Biophys Res Commun. 2009; 388:621–5. [PubMed: 19686699]
14. von Bernuth H, et al. Pyogenic bacterial infections in humans with MyD88 deficiency. Science. 2008; 321:691–6. [PubMed: 18669862]
15. Bousfiha A, et al. Primary immunodeficiencies of protective immunity to primary infections. Clin Immunol. 2010; 135:204–9. [PubMed: 20236864]
16. Martin TR, Frevert CW. Innate immunity in the lungs. Proc Am Thorac Soc. 2005; 2:403–11. [PubMed: 16322590]
17. Gozalo AS, et al. Spontaneous Staphylococcus xylosus Infection in Mice Deficient in NADPH Oxidase and Comparison with Other Laboratory Mouse Strains. J Am Assoc Lab Anim Sci. 49:480–6. [PubMed: 20819397]
18. Forlow SB, Foley PL, Ley K. Severely reduced neutrophil adhesion and impaired host defense against fecal and commensal bacteria in CD18−/−P-selectin−/− double null mice. FASEB J. 2002; 16:1488–96. [PubMed: 12374771]
19. Ostanin DV, Barlow S, Shukla D, Grisham MB. NADPH oxidase but not myeloperoxidase protects lymphopenic mice from spontaneous infections. Biochem Biophys Res Commun. 2007; 355:801–6. [PubMed: 17316569]
20. Tunney MM, et al. Detection of anaerobic bacteria in high numbers in sputum from patients with cystic fibrosis. Am J Respir Crit Care Med. 2008; 177:995–1001. [PubMed: 18263800]
21. Levy O. Innate immunity of the newborn: basic mechanisms and clinical correlates. Nat Rev Immunol. 2007; 7:379–90. [PubMed: 17457344]
22. Garvy BA, Harmsen AG. The importance of neutrophils in resistance to pneumococcal pneumonia in adult and neonatal mice. Inflammation. 1996; 20:499–512. [PubMed: 8894714]
23. Garvy BA, Qureshi MH. Delayed inflammatory response to Pneumocystis carinii infection in neonatal mice is due to an inadequate lung environment. J Immunol. 2000; 165:6480–6. [PubMed: 11086088]
24. Van Winkle LS, et al. Epithelial cell distribution and abundance in rhesus monkey airways during postnatal lung growth and development. J Appl Physiol. 2004; 97:2355–63. discussion 2354. [PubMed: 15298983]
25. Lamb D, Reid L. Acidic glycoproteins produced by the mucous cells of the bronchial submucosal glands in the fetus and child: a histochemical autoradiographic study. Br J Dis Chest. 1972; 66:248–53. [PubMed: 5083432]
26. Toskala E, Smiley-Jewell SM, Wong VJ, King D, Plopper CG. Temporal and spatial distribution of ciliogenesis in the tracheobronchial airways of mice. Am J Physiol Lung Cell Mol Physiol. 2005; 289:L454–459. [PubMed: 15879461]
27. Francis RJ, et al. Initiation and maturation of cilia-generated flow in newborn and postnatal mouse airway. Am J Physiol Lung Cell Mol Physiol. 2009; 296:L1067–75. [PubMed: 19346437]
28. Muhlebach MS, et al. Are lower airway or throat cultures predictive of sinus bacteriology in cystic fibrosis? Pediatr Pulmonol. 2006; 41:445–51. [PubMed: 16547960]

29. Bonestroo HJ, de Winter-de Groot KM, van der Ent CK, Arets HG. Upper and lower airway cultures in children with cystic fibrosis: do not neglect the upper airways. J Cyst Fibros. 9:130–4. [PubMed: 20110197]
30. Mainz JG, et al. Concordant genotype of upper and lower airways P aeruginosa and S aureus isolates in cystic fibrosis. Thorax. 2009; 64:535–40. [PubMed: 19282318]
31. Didierlaurent A, Goulding J, Hussell T. The impact of successive infections on the lung microenvironment. Immunology. 2007; 122:457–65. [PubMed: 17991012]
32. Craig A, Mai J, Cai S, Jeyaseelan S. Neutrophil recruitment to the lungs during bacterial pneumonia. Infect Immun. 2009; 77:568–75. [PubMed: 19015252]
33. Evans SE, Xu Y, Tuvim MJ, Dickey BF. Inducible innate resistance of lung epithelium to infection. Annu Rev Physiol. 72:413–35. [PubMed: 20148683]
34. Balamayooran T, Balamayooran G, Jeyaseelan S. Review: Toll-like receptors and NOD-like receptors in pulmonary antibacterial immunity. Innate Immun. 16:201–10. [PubMed: 20418253]
35. Le Bourhis L, et al. Antimicrobial activity of mucosal-associated invariant T cells. Nat Immunol. 11:701–8. [PubMed: 20581831]
36. Ricklin D, Hajishengallis G, Yang K, Lambris JD. Complement: a key system for immune surveillance and homeostasis. Nat Immunol. 11:785–97. [PubMed: 20720586]
37. Zola TA, Lysenko ES, Weiser JN. Natural antibody to conserved targets of Haemophilus influenzae limits colonization of the murine nasopharynx. Infect Immun. 2009; 77:3458–65. [PubMed: 19451240]
38. Silva MT, do Vale A, dos Santos NM. Secondary necrosis in multicellular animals: an outcome of apoptosis with pathogenic implications. Apoptosis. 2008; 13:463–82. [PubMed: 18322800]
39. Rowe SM, et al. Potential role of high-mobility group box 1 in cystic fibrosis airway disease. Am J Respir Crit Care Med. 2008; 178:822–31. [PubMed: 18658107]
40. Hilty M, et al. Disordered microbial communities in asthmatic airways. PLoS One. 5:e8578. [PubMed: 20052417]
41. Moghaddam SJ, et al. Haemophilus influenzae lysate induces aspects of the chronic obstructive pulmonary disease phenotype. Am J Respir Cell Mol Biol. 2008; 38:629–38. [PubMed: 18096867]
42. Hogg JC, et al. The nature of small-airway obstruction in chronic obstructive pulmonary disease. N Engl J Med. 2004; 350:2645–53. [PubMed: 15215480]
43. Machen TE. Innate immune response in CF airway epithelia: hyperinflammatory? Am J Physiol Cell Physiol. 2006; 291:C218–30. [PubMed: 16825601]
44. Bruscia EM, et al. Macrophages directly contribute to the exaggerated inflammatory response in cystic fibrosis transmembrane conductance regulator−/− mice. Am J Respir Cell Mol Biol. 2009; 40:295–304. [PubMed: 18776130]
45. Rogers CS, et al. Disruption of the CFTR gene produces a model of cystic fibrosis in newborn pigs. Science. 2008; 321:1837–41. [PubMed: 18818360]
46. Sun X, et al. Disease phenotype of a ferret CFTR-knockout model of cystic fibrosis. J Clin Invest. 120:3149–60. [PubMed: 20739752]
47. Wielputz MO, et al. In vivo monitoring of cystic fibrosis-like lung disease in mice by volumetric computed tomography. Eur Respir J. 38:1060–70. [PubMed: 21478215]
48. Adachi O, et al. Targeted disruption of the MyD88 gene results in loss of IL-1- and IL-18-mediated function. Immunity. 1998; 9:143–50. [PubMed: 9697844]
49. Durairaj L, et al. Safety assessment of inhaled xylitol in mice and healthy volunteers. Respir Res. 2004; 5:13. [PubMed: 15377394]

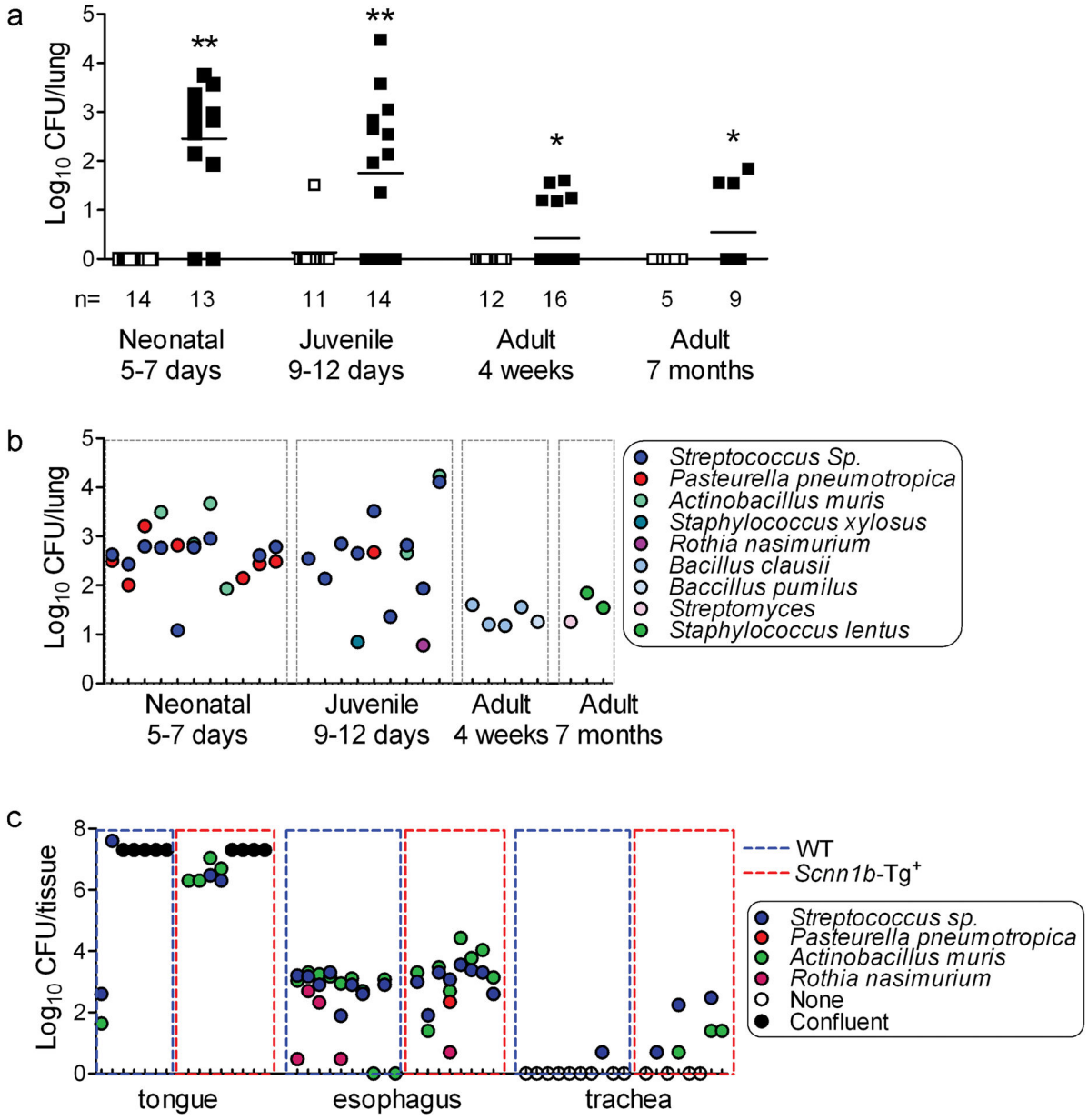

Figure 1. Spontaneous bacterial colonization in C57BL/6N *Scnn1b*-Tg$^+$ mice

(**a**) Timecourse analysis of total colony forming units (CFU) in BAL samples from *Scnn1b*-Tg$^+$ mice (■) and WT littermates (□). (Log_{10}+1)-transformed data. n= number of mice/group. T test ** $p<0.005$, * $p<0.05$ vs. WT littermates. (**b**) Individual CFUs and bacterial species isolated from C57BL/6N *Scnn1b*-Tg$^+$ mice. Each tick on the x axis represents an individual mouse. (**c**) Bacteria isolated from tongue, esophagus, trachea, and lung tissue homogenates of PND 5 C57BL/6N *Scnn1b*-Tg$^+$ mice and WT littermates. (Log_{10}+1)-transformed data. Each tick on the x axis represents an individual mouse. CFUs in confluent plates could not be enumerated and were arbitrarily set at 2×10^7 CFU/tissue.

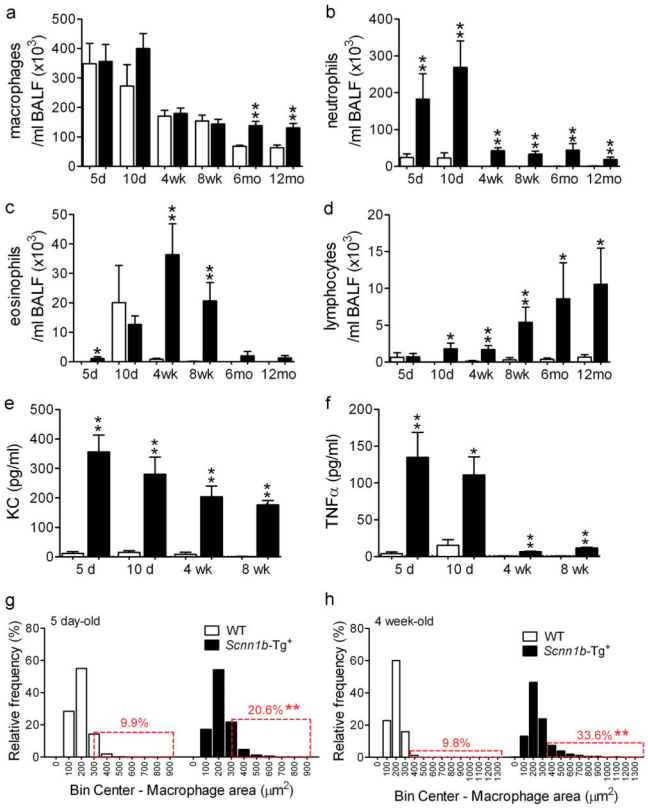

Figure 2. Developmental profile of lung inflammation in C57BL/6N *Scnn1b*-Tg$^+$ mice

(**a-d**). Longitudinal BAL cell counts in *Scnn1b*-Tg$^+$ mice (■) and WT littermates (□). n= 6 and 8 at 5 days (5d); n= 7 and 12 at 10 days (10d); n=12 and 13 at 4 weeks (4wk); n=10 and 8 at 8 weeks (8wk); n=4 and 4 at 6 months (6mo); n=14 and 6 at 12 months (12mo), for WT and *Scnn1b*-Tg$^+$, respectively. (**e-f**) Longitudinal KC and TNFα levels in BAL fluid. n= 4 WT and 6 *Scnn1b*-Tg$^+$ mice. T test ** p<0.005, * p<0.05 vs. WT littermates. (**g–h**) Macrophage size distribution in 5 day and 4 week-old C57BL/6N *Scnn1b*-Tg$^+$ mice and WT littermates. n= 6 WT and 8 *Scnn1b*-Tg$^+$ mice at PND 5; 10 WT and 13 *Scnn1b*-Tg$^+$ mice at PND 28. Boxed regions highlight the percentage of total macrophages larger than the 90th percentile in WT mice. T test ** p<0.005, * p<0.05 vs. WT littermates.

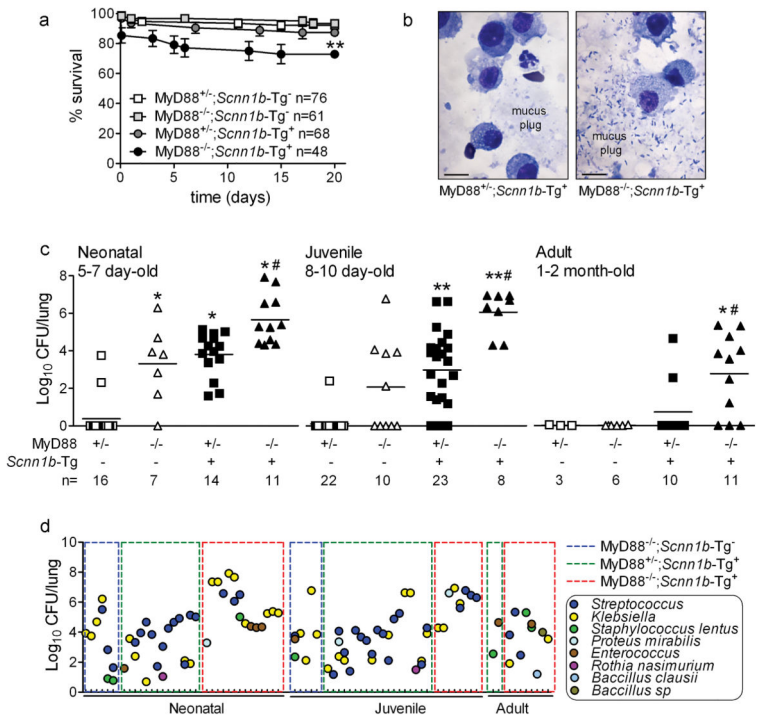

Figure 3. Genetic deletion of MyD88 decreases neonatal survival and increases lung bacterial burden in WT and *Scnn1b*-Tg$^+$ mice

(**a**) Survival curves. Absence of MyD88 in *Scnn1b*-Tg$^+$ mice lowers survival. ANOVA * p = 0.004 vs. littermates. **(b)** Representative photomicrograph of BAL cytospin preparations from neonatal MyD88-sufficient and -deficient *Scnn1b*-Tg$^+$ mice, illustrating mucus-associated bacteria in MyD88$^{-/-}$;*Scnn1b*-Tg$^+$ mice. Scale bar = 10 μm. (**c**) Bacterial CFU in mice from the MyD88$^{-/-}$ × *Scnn1b*-Tg$^+$ cross at the ages indicated, (Log_{10}+1)-transformed data. n= number of mice/group. ANOVA ** p<0.005, * p<0.05 vs. MyD88$^{+/-}$;*Scnn1b*-Tg$^-$ mice. # p<0.05 vs. MyD88$^{+/-}$;*Scnn1b*-Tg$^+$ mice. (d) Lung microflora in mice from the MyD88$^{-/-}$ × *Scnn1b*-Tg$^+$ cross. Each tick on the x axis represents an individual mouse.

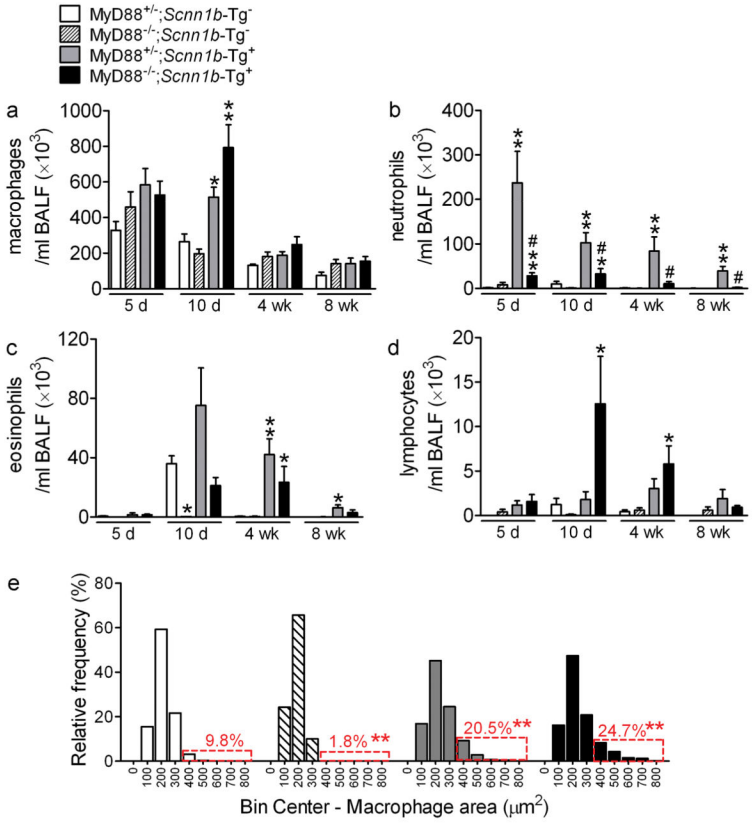

Figure 4. Genetic deletion of MyD88 reduces lung neutrophilia in *Scnn1b*-Tg$^+$ mice, but does not blunt macrophage activation

(**a–d**) Differential BAL cell counts. n= 8, 9, 8, 8 at 5 days (5d), n= 14, 9, 12, 12 at 10 days (10d), n= 5, 5, 5, 9 at 4 weeks (4wk), and n= 3, 6, 7, 8 at 8 weeks (8wk) for MyD88$^{+/-}$;*Scnn1b*-Tg$^-$, MyD88$^{-/-}$;*Scnn1b*-Tg$^-$, MyD88$^{+/-}$;*Scnn1b*-Tg$^+$, and MyD88$^{-/-}$;*Scnn1b*-Tg$^+$ mice, respectively. ANOVA ** p<0.005, * p<0.05 vs. MyD88$^{+/-}$;*Scnn1b*-Tg$^-$ mice. # p<0.05 vs. MyD88$^{+/-}$;*Scnn1b*-Tg$^+$ mice. (**e)** Macrophage size distribution in 4 week-old mice from the MyD88$^{-/-}$ × *Scnn1b*-Tg$^+$ cross. Boxed regions highlight the percentage of total macrophages larger than the 90th percentile in MyD88$^{+/-}$;*Scnn1b*-Tg$^-$ mice. n=5 MyD88$^{+/-}$;*Scnn1b*-Tg$^-$, 4 MyD88$^{-/-}$;*Scnn1b*-Tg$^-$, 5 MyD88$^{+/-}$;*Scnn1b*-Tg$^+$, and 8 MyD88$^{-/-}$;*Scnn1b*-Tg$^+$. ANOVA ** p<0.005, * p<0.05 vs. MyD88$^{+/-}$;*Scnn1b*-Tg$^-$littermates.

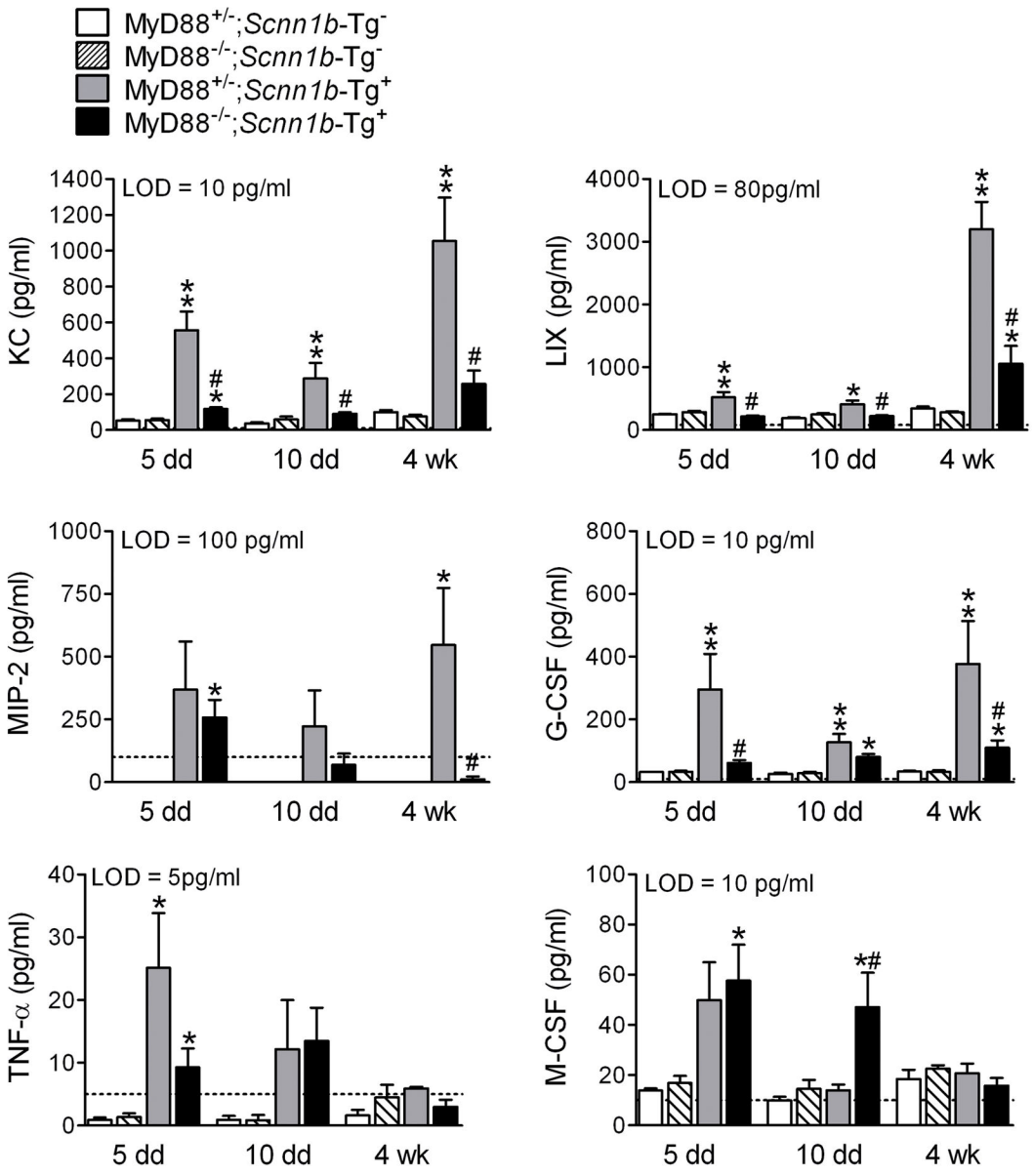

Figure 5. MyD88 deletion in *Scnn1b*-Tg$^+$ mice alters BAL neutrophil- and macrophage-related inflammatory mediators

BAL cytokines in 5 day-, 10 day- and 4 week-old mice. The dotted line represents the assay lower detection limit (LOD). n = 4 for WT mice and n=6 for *Scnn1b*-Tg$^+$ mice. ANOVA ** $p<0.005$, * $p<0.05$ vs. age-matched MyD88$^{+/-}$;*Scnn1b*-Tg$^-$ mice. # $p<0.05$ vs. MyD88$^{+/-}$;*Scnn1b*-Tg$^+$ mice.

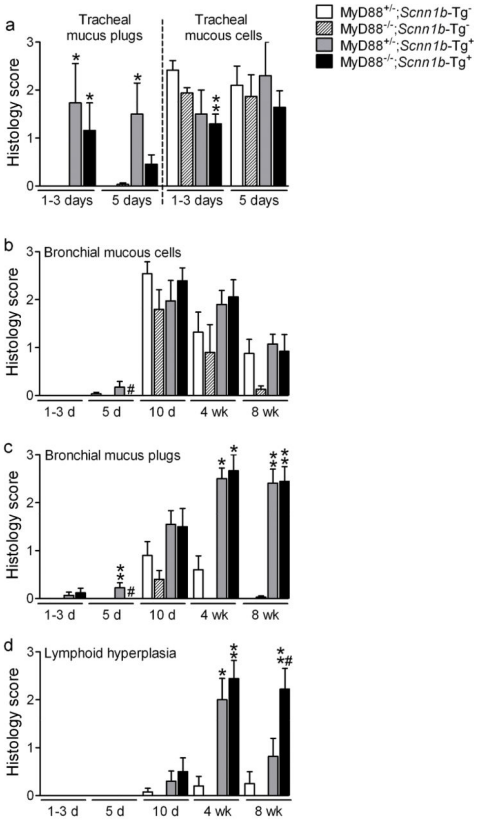

Figure 6. MyD88 deletion does not modify mucus plugging, but promotes development of lymphoid aggregates in *Scnn1b*-Tg$^+$ mice

(**a-c**)Semi-quantitative histopathology scores for mucus plugs and mucous secretory cells (AB-PAS positive) in (**a**) neonatal trachea and (b-c) left lobe intrapulmonary main stem bronchus, at different time points. (**d**) Semi-quantitative histopathology scores for lymphoid aggregates (BALT). n= 6, 8, 3, 5 at 1–3 days (1–3d), n= 5, 6, 4, 8 at 5 days (5d), n= 13, 5, 10, 12 at 10 days (10d), n= 5, 4, 5, 9 at 4 weeks (4wk), and n= 8, 8, 11, 9 at 8 weeks (8wk) for MyD88$^{+/-}$;*Scnn1b*-Tg$^-$; MyD88$^{-/-}$;*Scnn1b*-Tg$^-$; MyD88$^{+/-}$;*Scnn1b*-Tg$^+$; and MyD88$^{-/-}$;*Scnn1b*-Tg$^+$ mice, respectively. ANOVA ** $p<0.005$, * $p<0.05$ vs. MyD88$^{+/-}$;*Scnn1b*-Tg$^-$ mice. # $p<0.05$ vs. MyD88$^{+/-}$;*Scnn1b*-Tg$^+$ mice.

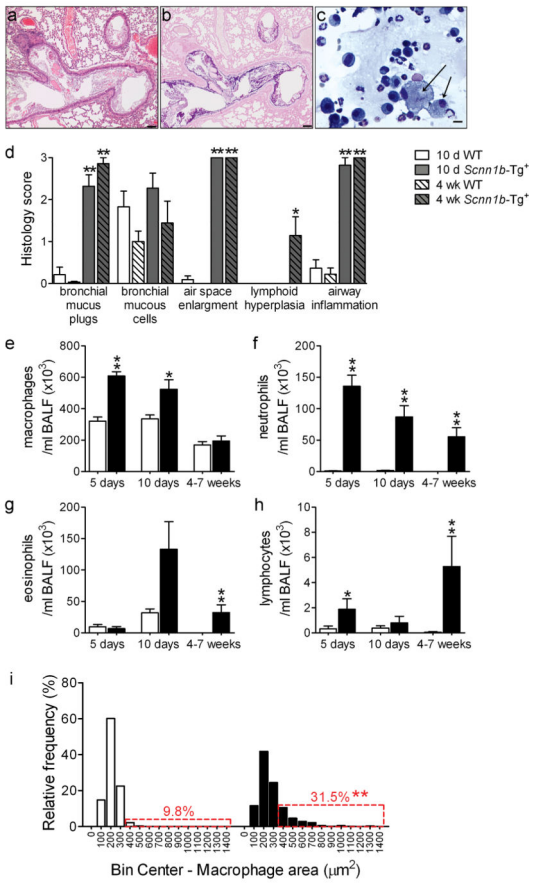

Figure 7. Germ-free (GF) *Scnn1b*-Tg$^+$ mice develop lung inflammation similar to *Scnn1b*-Tg$^+$ mice raised in conventional SPF conditions

(**a, b**) Representative photomicrographs of left lobe main stem bronchus from 6 week-old GF *Scnn1b*-Tg$^+$ mice, illustrating alveolar space enlargement, mucus obstruction, and airway inflammation. H&E (**a**) and AB-PAS (**b**) stain. Scale bar 100 μm. (**c**) Representative photomicrograph of BAL cytospin preparation from GF *Scnn1b*-Tg$^+$ mice, illustrating mucus plugs (light blue), granulocytes and large/foamy macrophages (arrows). Giemsa stain, scale bar = 20 μm. (**d**) Semi-quantitative histopathology scores for 10 day old (10 d, open bars) and 4 week-old (4 wk, hatched bars) *Scnn1b*-Tg$^+$ mice (gray) and WT littermates (white) raised in GF conditions, n= 11 *Scnn1b*-Tg$^+$ and 11 WT littermates at 10 days, n=7 *Scnn1b*-Tg$^+$ and 9 WT littermates at 4 weeks of age. T test ** $p<0.005$, * $p<0.05$ vs. WT littermates. (**e-h**) Longitudinal differential BAL cell counts for GF *Scnn1b*-Tg$^+$ mice (■) and WT littermates (□). n= 11 and 11 at 5 days, n= 18 and 8 at 10 days, n= 8 and 7 at 4–7 weeks, for GF WT and GF *Scnn1b*-Tg$^+$ mice, respectively. (**i**) Macrophage size distribution in 4–7 week-old GF *Scnn1b*-Tg$^+$ mice (■, n=7) and WT littermates (□, n=8). Boxed regions highlight the percentage of total macrophages larger than the 90th percentile in WT mice. T test ** $p<0.005$ vs. WT littermates.

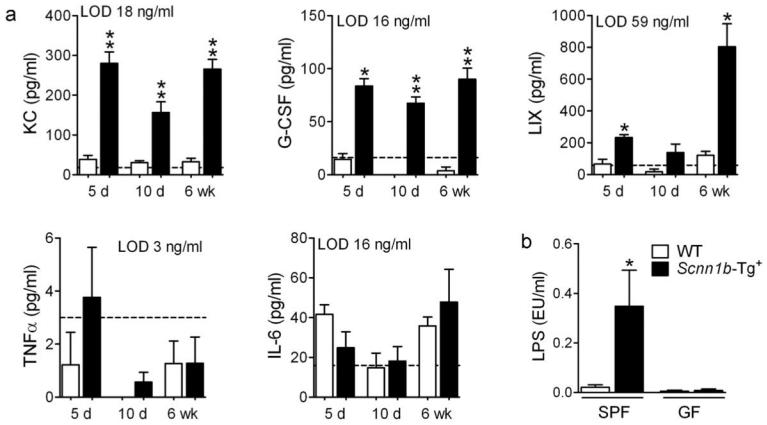

Figure 8. BAL cytokine profile and BAL LPS content in germ-free *Scnn1b*-Tg$^+$ mice and WT littermates

(**a**) BAL cytokines in 5 day-, 10 day- and 6 week-old mice. The dotted line represents the assay lower detection limit (LOD). n = 6 for WT and 8 for *Scnn1b*-Tg$^+$ mice. ANOVA ** $p<0.005$, * $p<0.05$ vs. WT littermates. (**b**) LPS content in BAL isolated from SPF or GF *Scnn1b*-Tg$^+$ mice (■) and WT littermates (□). n= 14 and 11 for SPF WT and *Scnn1b*-Tg$^+$ mice, respectively; n= 4 and 5 for GF WT and *Scnn1b*-Tg$^+$ mice, respectively. T test * $p<0.05$ vs. WT littermates.